© 2022. Published by The Company of Biologists Ltd | Development (2022) 149, dev200775. doi:10.1242/dev.200775

RESEARCH REPORT

C. elegans srGAP is an α-catenin M domain-binding protein that strengthens cadherin-dependent adhesion during morphogenesis

Joel M. Serre[1], Bethany Lucas[2], Sterling C. T. Martin[3], Jonathon A. Heier[4], Xiangqiang Shao[5] and Jeff Hardin[1,3,4,*]

ABSTRACT

The cadherin-catenin complex (CCC) is central to embryonic development and tissue repair, yet how CCC binding partners function alongside core CCC components remains poorly understood. Here, we establish a previously unappreciated role for an evolutionarily conserved protein, the slit-robo GTPase-activating protein SRGP-1/srGAP, in cadherin-dependent morphogenetic processes in the *Caenorhabditis elegans* embryo. SRGP-1 binds to the M domain of the core CCC component, HMP-1/α-catenin, via its C terminus. The SRGP-1 C terminus is sufficient to target it to adherens junctions, but only during later embryonic morphogenesis, when junctional tension is known to increase. Surprisingly, mutations that disrupt stabilizing salt bridges in the M domain block this recruitment. Loss of SRGP-1 leads to an increase in mobility and decrease of junctional HMP-1. In sensitized genetic backgrounds with weakened adherens junctions, loss of SRGP-1 leads to late embryonic failure. Rescue of these phenotypes requires the C terminus of SRGP-1 but also other domains of the protein. Taken together, these data establish a role for an srGAP in stabilizing and organizing the CCC during epithelial morphogenesis by binding to a partially closed conformation of α-catenin at junctions.

KEY WORDS: SrGAP, α-Catenin, Cadherin complex, *C. elegans*, Morphogenesis, Cell-cell adhesion

INTRODUCTION

As cells rearrange and change shape during embryonic morphogenesis, adhesions between cells must be dynamically formed, broken and reformed (Pinheiro and Bellaiotache, 2018; Takeichi, 2014; Walck-Shannon and Hardin, 2014), yet they must also withstand tensile forces (Charras and Yap, 2018; Guillot and Lecuit, 2013; Leckband and de Rooij, 2014; Lecuit and Yap, 2015; Pannekoek et al., 2019; Priya and Yap, 2015). Central to meeting this fundamental challenge is the cadherin-catenin complex (CCC) (Harris and Tepass, 2010; Leckband and de Rooij, 2014; Lecuit and Yap, 2015; Niessen et al., 2011; Takeichi, 2014). The CCC mediates intercellular adhesion at adherens junctions (AJs) through homophilic interactions of transmembrane cadherins. β-Catenin binds the cadherin C terminus and the N terminus of α-catenins (Pokutta and Weis, 2007). The C terminus of α-catenin binds F-actin, linking the CCC to the cytoskeleton (Buckley et al., 2014; Maiden and Hardin, 2011; Mege and Ishiyama, 2017).

The CCC must respond to differing tension states (Charras and Yap, 2018; Guillot and Lecuit, 2013; Huveneers and de Rooij, 2013; Leckband and de Rooij, 2014; Lecuit et al., 2011; Lecuit and Yap, 2015; Mege and Ishiyama, 2017). α-Catenin is one locus for such regulation. Imaging (Kim et al., 2015), molecular dynamics simulations (Barrick et al., 2018; Ishiyama et al., 2018; Li et al., 2015), crystallographic data (Choi et al., 2012; Ishiyama et al., 2013, 2018; Kang et al., 2017) and single-molecule tweezing (Pang et al., 2019; Yao et al., 2014) suggest that the middle (M) domain of α-catenins undergoes reversible distension under tension. Tension unmasks the binding site for vinculin in vertebrate αE-catenin (Yonemura et al., 2010); however, disruption of vinculin binding sites in αE-catenin leads to weak effects (Huveneers et al., 2012), suggesting that additional tension-sensitive α-catenin binding partners may act cooperatively to strengthen the CCC.

A useful system for identifying novel, functionally relevant, interactors with the CCC is the embryonic epidermis of the *Caenorhabditis elegans* embryo. The epidermis is born on the dorsal side of the embryo and spreads ventrally during ventral enclosure (Williams-Masson et al., 1997). After enclosure, actomyosin-mediated constriction of epidermal cells squeezes the embryo into a vermiform shape (Chisholm and Hardin, 2005; Marston and Goldstein, 2006; Vuong-Brender et al., 2016). In *C. elegans*, the core CCC is composed of HMR-1/cadherin, HMP-1/α-catenin, and HMP-2/β-catenin (see Fig. S1A). Maternal loss of CCC components leads to ventral enclosure failure; zygotic loss results in failure of elongation due to defects in the junctional proximal actin network (Costa et al., 1998; Kwiatkowski et al., 2010; Maiden et al., 2013; Vuong-Brender et al., 2018).

We previously used a weak loss-of-function allele of *hmp*-1 to look for synergistic, lethal enhancers of morphogenetic defects during embryonic morphogenesis (Cox-Paulson et al., 2012; Lynch et al., 2012). One of these is the single *C. elegans* slit-robo GTPase activating protein (srGAP) homolog SRGP-1 (Zaidel-Bar et al., 2010). srGAPs have an N-terminal, lipid-binding, extended F-BAR domain (Coutinho-Budd et al., 2012; Guez-Haddad et al., 2015; Sporny et al., 2017); a GTPase-activating protein (GAP) domain that can downregulate Rho family GTPases (Foletta et al., 2002; Guerrier et al., 2009; Liang et al., 2017; Mason et al., 2011; Soderling et al., 2002; Waltereit et al., 2012; Wong et al., 2001; Yamazaki et al., 2013; Yang et al., 2006); and a C-terminal SH3 domain that binds F-actin regulators (Carlson et al., 2011; Endris et al., 2011).

Here, we use a combination of genetic, biochemical and imaging approaches in *C. elegans* to demonstrate a role for SRGP-1 in binding a closed conformation of the HMP-1 M domain to stabilize

[1]Program in Genetics, University of Wisconsin-Madison, Madison, WI 53706, USA. [2]Department of Biology, Regis University, 3333 Regis Blvd., Denver, CO 80221, USA. [3]Biophysics Graduate Program, University of Wisconsin-Madison, Madison, WI 53706, USA. [4]Department of Integrative Biology, University of Wisconsin-Madison, Madison, WI 53706, USA. [5]Wisconsin State Laboratory of Hygiene, University of Wisconsin-Madison, Madison, WI 53706, USA.

*Author for correspondence (jdhardin@wisc.edu)

J.H., 0000-0001-7399-6580

Handling Editor: Thomas Lecuit
Received 23 March 2022; Accepted 23 August 2022

Development (2022) 149, dev200775. doi:10.1242/dev.200775

adherens junctions under mechanical tension during embryonic morphogenesis.

RESULTS AND DISCUSSION

SRGP-1 binds HMP-1

SRGP-1 is a bona fide srGAP based on homology and structure-function analyses ((Neukomm et al., 2011; Zaidel-Bar et al., 2010; see Fig. 1C). SRGP-1 colocalizes with the CCC, and when SRGP-1::GFP is overexpressed outward membrane bends form that contain CCC proteins but not DLG/AJM complex proteins (Zaidel-Bar et al., 2010). We also identified SRGP-1 in an HMP-1 co-immunoprecipitation/mass spectrometry screen (Callaci et al., 2015). We verified this result (Fig. 1A) and used a yeast two-hybrid assay to show that full-length SRGP-1 can interact directly with full-length HMP-1 but not HMP-2/β-catenin (Fig. 1B). We confirmed this interaction via protein pull-down assays using His-SUMO-HMP-1 (Callaci et al., 2015) and GST-SRGP-1 in bacteria. Using a series of deletions (for domain maps, see Fig. 1C), we found that the HMP-1M domain appears to be responsible for the interaction with amino acids 685-1059 of SRGP-1 (hereafter the 'C terminus'; Fig. 1D, Fig. S1B).

SRGP-1 is maintained at the junction during morphogenesis through its C terminus

We next assessed the necessity of the SRGP-1 C terminus for SRGP-1 colocalization with HMP-1 *in vivo*. SRGP-1(ΔC)::GFP exhibits a marked increase in cytoplasmic versus junctional signal compared with full-length SRGP-1 (Fig. 1E,F). Both proteins contain an intact F-BAR domain, and so, as expected, readily associate with and follow the curvature of the membrane. Full-length SRGP-1::GFP and HMP-1::mScarlet-I closely followed the curvature of the membrane at junctions. In contrast, HMP-1 frequently no longer followed SRGP-1(ΔC)::GFP into membrane bends (Fig. 1F, insets), as reflected in a change in overlap at junctions in 1.5-fold embryos (Manders overlap coefficient M2 with thresholding; GFP overlap with mScarlet-I=0.82 for SRGP-1::GFP, n=57 junctions; M2=0.46 for SRGP-1(ΔC)::GFP, n=36). These data indicate that the SRGP-1 C-terminus is necessary for restricting SRGP-1 to junctions and for normal association with HMP-1. Because some SRGP-1ΔC can localize to junctions, we infer that additional interactions outside the C terminus also promote accumulation of SRGP-1 at junctions.

We next determined whether the C terminus is sufficient to target SRGP-1 to the CCC. Full-length SRGP-1::GFP expressed in the *srgp-1(gk441841)* null background was robustly targeted to cell-cell junctions throughout morphogenesis (Fig. 2A). In contrast, SRGP-1(C term)::GFP failed to localize in the early embryo; SRGP-1(C term)::GFP remained much more cytoplasmic in later embryos, but localized to junctions during ventral enclosure and elongation (Fig. 2B, yellow arrows).

We next assessed the effects of HMP-1 depletion on SRGP-1 junctional recruitment. SRGP-1::GFP was not depleted from induced membrane tubulations in *hmp-1(RNAi)* embryos (Fig. 2C, right, yellow arrowheads), but junctional SRGP-1 was greatly reduced (see Fig. 2E for quantification), indicating that HMP-1 is required for normal junctional recruitment of SRGP-1 during morphogenesis. In contrast, *hmp-1(RNAi)* led to complete loss of junctional SRGP-1(C term) at all stages (Fig. 2D,E), indicating that interaction of the SRGP-1 C terminus with the CCC has a stringent requirement for HMP-1.

The HMP-1M domain is required for normal SRGP-1 recruitment

Our previous work showed that expression of a construct lacking most of the HMP-1M domain [HMP-1(ΔVH2)::GFP] can rescue viability, albeit weakly, in embryos carrying a C-terminal HMP-1 truncation, *hmp-1(zu278)* (Maiden et al., 2013). It remained possible, however, that other parts of the HMP-1M domain retained in *zu278* mutants recruit other interactors. We confirmed that the same M domain deletion can partially rescue *hmp-1* CRISPR null (*jc48*) homozygotes (Shao et al., 2019) from 100% to 35.3% embryonic lethality (Fig. 2G).

We next examined the effects of deletion of the HMP-1M domain on SRGP-1 recruitment. *srgp-1::mScarlet-I; hmp-1(jc48); Ex[hmp-1(ΔVH2)::gfp]* embryos retained detectable membrane-localized SRGP-1::mScarlet-I in lateral epidermal cells (seam cells) during elongation but at greatly reduced levels (Fig. 2F,H,I). Thus, the HMP-1M domain appears to be important for recruiting or maintaining SRGP-1 at the CCC during embryonic elongation.

Recruitment of the SRGP-1 C terminus depends on the conformation of the HMP-1M domain

Our previous structural work (Kang et al., 2017) demonstrated that HMP-1 possesses conserved salt bridges that are structural analogs of salt bridges in mammalian αE-catenin (Barrick et al., 2018; Li et al., 2015). Two arginines (R551 and R554) in the MIII subdomain are predicted to stabilize the internal structure of the HMP-1M domain, resisting its complete extension by forming salt bridges with two residues (D386 and D497, respectively) in the MII subdomain. We used CRISPR/Cas9 mutagenesis to mutate these arginines to alanines. Limited proteolysis has been used to assess the conformational openness of α-catenin (Heier et al., 2021; Pokutta and Weis, 2000; Xu et al., 2020); limited proteolysis of HMP-1 similarly indicates that the D386A and D497A mutations led to an open conformation of the HMP-1M domain (Fig. S2A,B). *hmp-1(R551/554A)::mScarlet-I* mutants were viable and did not display overt morphological defects under laboratory conditions. We then constructed *srgp-1(gk441841);hmp-1(R551/554A)::mScarlet-I* strains expressing *srgp-1::gfp* constructs. Whereas full-length HMP-1::mScarlet-I colocalized precisely with full-length SRGP-1::GFP (Fig. 3A, top), HMP-1(R551/554A) did not (Fig. 3A, second row), reflected in a statistically significant decrease in colocalization at junctions [Pearson's r=0.53 for HMP-1::mScarlet-I versus SRGP-1::GFP pixels above threshold, n=25 junctions; r=0.49 for HMP-1(R551/554A)::mScarlet-I versus SRGP-1::GFP, n=25; P<0.0001, unpaired Student's t-test]. The SRGP-1 C terminus is enriched at seam-seam junctions (Fig. 3A, blue dashed line) compared with seam-non-seam junctions (Fig. 3A, yellow dashed line) during elongation. Weak RNAi against *let-502/ROCK*, an activator of actomyosin contractility, resulted in increased recruitment of SRGP-1(C-term)::GFP to seam-non-seam junctions (Figs S2C,D). Strikingly, junctional enrichment of SRGP-1(C term)::GFP was completely abrogated in *hmp-1(R551/554A)::mScarlet-I* embryos (Fig. 3A bottom row; quantified in Fig. 3B). These results indicate that junctional recruitment of the SRGP-1 C terminus requires the HMP-1M domain to be in a partially closed conformation. Weak knockdown of *let-502*/ROCK presumably leads to a decrease in the fraction of HMP-1 protein in a fully extended state at seam-non-seam junctions, which are under high tension during elongation (Costa et al., 1998; Cox-Paulson et al., 2012; Vuong-Brender et al., 2017, 2018), thereby allowing recruitment of the SRGP-1 C terminus.

Normal levels and mobility of HMP-1 at junctions require SRGP-1 function

We next examined whether SRGP-1 is required for normal junctional morphology. We could not detect a statistically significant effect on

Development (2022) 149, dev200775. doi:10.1242/dev.200775

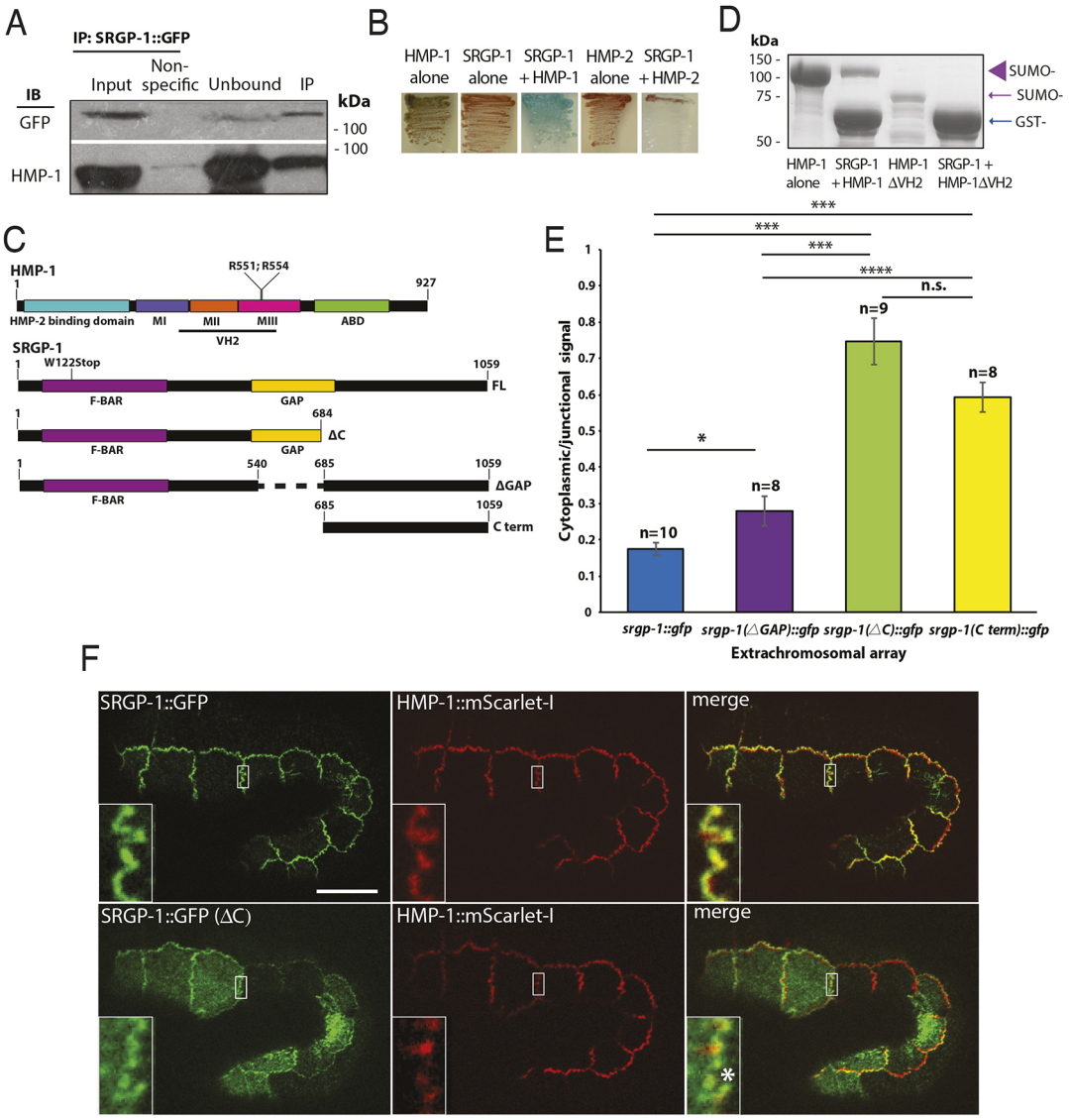

Fig. 1. SRGP-1 and HMP-1 interact *in vitro* and *in vivo*. (A) Co-immunoprecipitation of HMP-1 and SRGP-1::GFP from mixed-stage embryos, larvae and adults. 'Non-specific' refers to lysate bound to protein-G agarose beads without antibody present; 'unbound refers to protein that did not immunoprecipitate. (B) Yeast two-hybrid assay showing direct interaction between full-length HMP-1 and full-length SRGP-1 (blue) but not between full-length HMP-2 and full-length SRGP-1 (brown). Brown color indicates no autoactivation in yeast transformed with single constructs. (C) Protein domain structures of SRGP-1 and HMP-1 with relevant mutations indicated and deletion constructs used in this study. (D) Protein pull-down between full-length SUMO-HMP-1 (purple arrowhead) or SUMO-HMP-1(ΔVH2) (purple arrow) and GST-SRGP-1(C term) (blue arrow). GST-SRGP-1(C term) interacts with full-length HMP-1, but not SUMO-HMP-1(ΔVH2). Additional pull-downs with deletions are shown in Fig. S2. (E) Cytoplasmic versus junctional localization of SRGP-1 (mean±s.e.m.). ns, not significant; *P<0.05, ***P<0.001, ****P<0.0001 (ANOVA with Tukey post-hoc test). (F) SRGP-1::GFP deletions lacking the C terminus do not retain normal colocalization with HMP-1 at sites of membrane bending. Top: Full-length SRGP-1::GFP (green), HMP-1::mScarlet-I (red), and merge. Insets show higher magnification views of a junction between a seam (lateral) and dorsal epidermal cell. Colocalization of HMP-1 and SRGP-1 occurs in SRGP-1-induced membrane bends. Bottom: SRGP-1(ΔC)::GFP (green), HMP-1::mScarlet-I (red), and merge. Insets show higher magnification views. HMP-1 no longer consistently colocalizes with SRGP-1::GFP(ΔC) in membrane bends. Asterisk indicates a tubulation without HMP-1. Scale bar: 10 µm.

junctional tortuosity (total path length/Feret length) in *srgp-1(gk441841)* embryos (wild-type ratio=1.24, n=43; *gk441841* ratio=1.23, n=33; P>0.76, two-tailed Student's t-test). We did find, however, that in *srgp-1*(*gk441841*) mutants the average junctional intensity of an endogenous HMP-1::GFP knock-in (Marston et al., 2016) was measurably decreased compared with wild type (Fig. 3C). HMP-1(R551/554A)::GFP showed a similar decrease in junctional intensity (Fig. 3C). We next analyzed mobility of HMP-1 at junctions in 1.5- to 1.75-fold embryos using fluorescence recovery after photobleaching (FRAP; Fig. 3D). Loss of SRGP-1 led to a statistically significant decrease in recovery half-life ($t_{1/2}$ for wild type=25.0 s; $t_{1/2}$ for *srgp-1*=30.5 s; P<0.04, unpaired two-tailed Student's t-test, n=11 for each), indicating increased mobility of HMP-1 in the absence of SRGP-1. These results suggest a reciprocal role for SRGP-1 in organizing and stabilizing HMP-1 at junctions.

The SRGP-1 C terminus is required in CCC-sensitized backgrounds

srgp-1(RNAi) in the *hmp-1* weak loss-of-function mutant *hmp-1(fe4[S823F])* causes many embryos to arrest with defects in gastrulation cleft closure and subsequent ventral enclosure (Zaidel-Bar et al., 2010). We analyzed the remaining

Development (2022) 149, dev200775. doi:10.1242/dev.200775

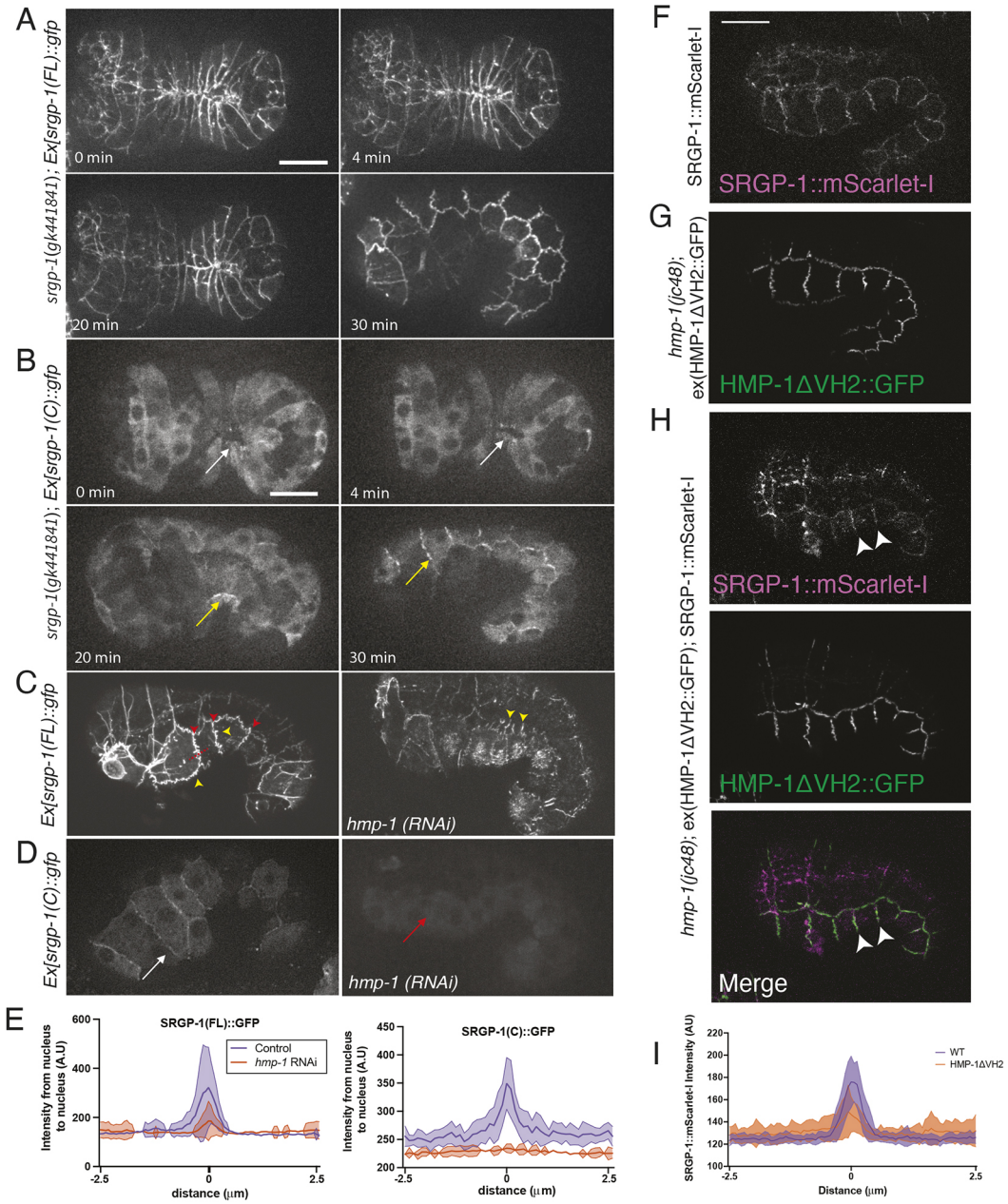

Fig. 2. Junctional maintenance of SRGP-1 requires HMP-1. (A) SRGP-1(full-length)::GFP expression in mutants lacking endogenous SRGP-1. Scale bar: 10 µm. (B) SRGP-1(C term)::GFP expression in mutants lacking endogenous SRGP-1. During ventral enclosure, SRGP-1(C term)::GFP is not localized to cell-cell junctions, or at the leading edge (white arrows). As the ventral midline seals and the embryo begins to elongate, SRGP-1(C term)::GFP localizes to junctions (20 and 30 min, yellow arrows). Scale bar: 10 µm. (C) Left: Overexpression of SRGP-1::GFP in a wild-type background leads to strong junctional expression (red arrowheads) and junction-associated membrane extensions (yellow arrowheads). Right: Depletion of HMP-1 by injection RNAi dramatically reduces junctional localization of SRGP-1 but does not deplete full-length SRGP-1::GFP from apical membrane extensions (yellow arrowheads). (D) Left: SRGP-1(C term)::GFP expressed in a wild-type embryo localizes to cell-cell junctions during elongation (white arrow). Right: SRGP-1(C term)::GFP is no longer recruited and/or maintained at the junction in *hmp-1(RNAi)* embryos (red arrow). (E) Intensity profiles showing SRGP-1::GFP intensity along a 5 µm line centered on the junction (red line in B indicates an example site of measurement) in control (purple) and *hmp-1* RNAi (orange) backgrounds for full-length SRGP-1 (left) and C terminus only (right). Dark lines indicate mean value; shaded areas indicate s.d. SRGP-1(FL)::GFP control: *n*=9 measurements; *hmp-1* RNAi: *n*=16. SRGP-1(C)::GFP control: *n*=7; *hmp-1* RNAi: *n*=14. (F) In *srgp-1::mScarlet-I* embryos, SRGP-1::mScarlet-I accumulates at junctions during elongation. Scale bar: 10 µm. (G) *hmp-1(jc48); Ex[hmp-1(ΔVH2)::gfp)]* embryos are viable and can appear largely wild type. (H) SRGP-1::mScarlet-I; *hmp-1(jc48); Ex[hmp-1(ΔVH2)::gfp)]* embryos show reduced SRGP-1::mScarlet-I junctional accumulation, although small amounts of SRGP-1::mScarlet-I can still accumulate at sites of cell-cell contact during elongation (white arrowheads). (I) HMP-1 intensity profiles (as in E) for wild type (WT) (purple) and HMP-1ΔVH2::GFP (orange). WT, *n*=25 measurements; HMP-1ΔVH2::GFP, *n*=24.

hmp-1(fe4); *srgp-1(RNAi)* embryos that survived beyond ventral enclosure. *hmp-1(fe4); srgp-1(RNAi)* embryos arrested as they approached the 2-fold stage of elongation with pronounced dorsal folds (100% of embryos, *n*=21 embryos; see Fig. 3E; Movie 1); thus, SRGP-1 also plays key roles during early stages of embryonic elongation.

We were unable to create *srgp-1(gk441841); hmp-1(fe4)* double mutants for rescue experiments, likely because *fe4* is a maternal

Development (2022) 149, dev200775. doi:10.1242/dev.200775

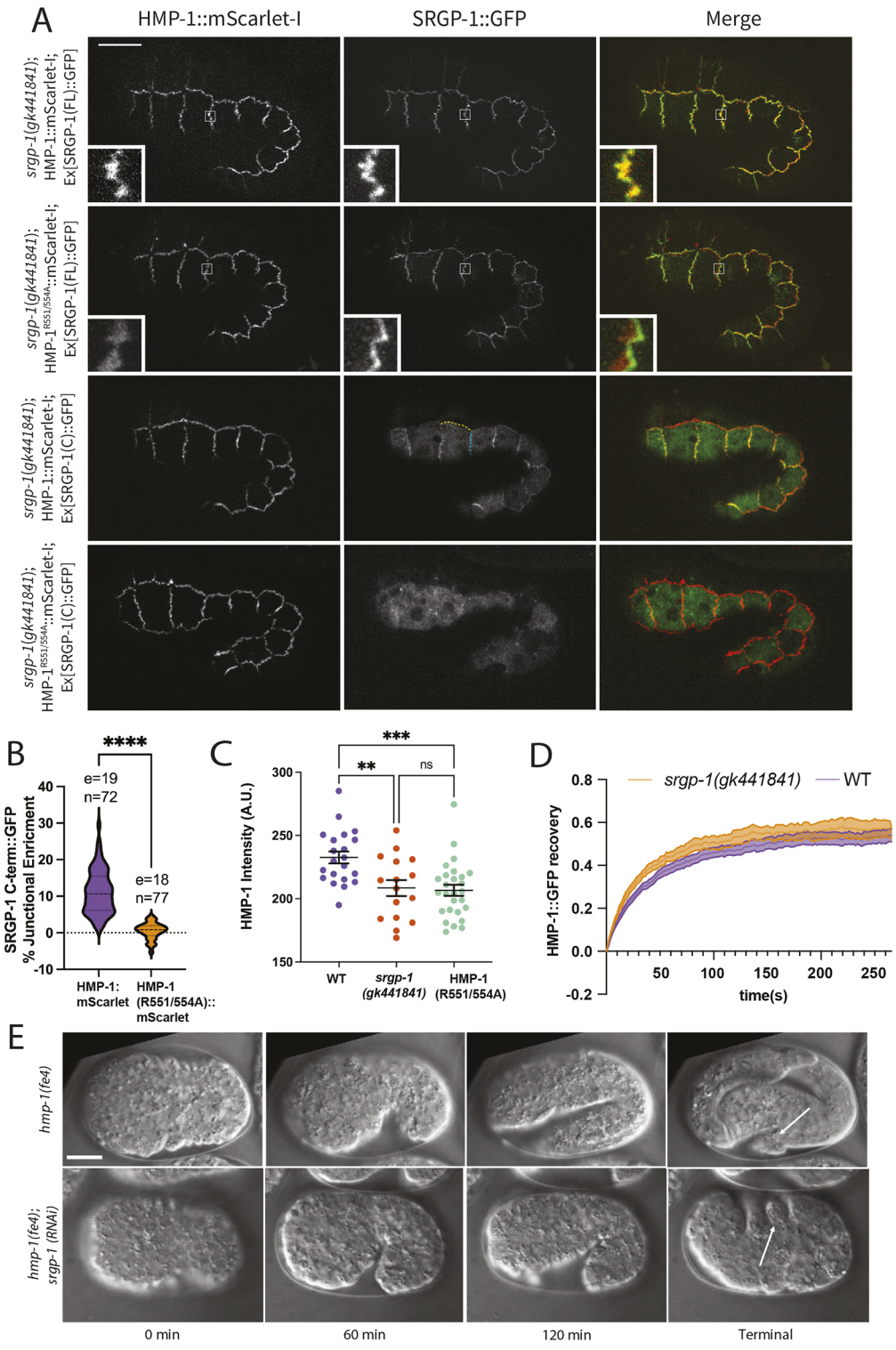

Fig. 3. Salt bridges within the HMP-1M domain are required for recruitment of the SRGP-1 C terminus. (A) Top row: SRGP-1::GFP colocalization with HMP-1::mScarlet-I. Scale bar: 10 µm. Second row: SRGP-1::GFP colocalization with HMP-$1^{R551/554A}$::mScarlet-I. Insets in the first and second row are magnified images of the junctions indicated by boxes. Third row: SRGP-1(C-term)::GFP colocalization with HMP-1::mScarlet-I. Blue dotted line indicates seam-seam junction, yellow dotted line indicates seam-non-seam junction. Bottom row: SRGP-1(C-term)::GFP localization with HMP-$1^{R551/554A}$::mScarlet-I. (B) Violin plot of percentage enrichment of SRGP-1(C)::GFP at junctions. ****P<0.0001 (unpaired Student's t-test). e, embryos; n, junctions analyzed. (C) HMP-1::GFP average intensity in wild-type (WT), *srgp-1(gk441841)* and HMP-$1^{R551/554A}$::GFP backgrounds. WT: n=21; *srgp-1*(gk441841): n=16; HMP-1(R551/554A): n=27. ns, not significant; **P<0.01, ***P<0.001 (ANOVA, Tukey post-hoc test). (D) FRAP for HMP-1::GFP in WT and *srgp-1(gk441841)* (n=11 for each genotype). Central line represents normalized mean intensity and shaded area represents s.e.m. (E) DIC images of representative *hmp-1(fe4)* and *hmp-1(fe4); srgp-1(RNAi)* embryos from ventral enclosure through elongation. Scale bar: 10 µm.

effect allele (J. Pettitt, personal communication) instead, we used homozygotes for a hypomorphic allele of *hmp-2*/β-catenin, *hmp-2(qm39)* (Lockwood et al., 2008; Zaidel-Bar et al., 2010) as a sensitized background. *hmp-2(qm39)* embryos appeared largely wild type during embryonic development, but later developed slight body morphology defects that resolved during cuticle molts (Fig. 4A). In contrast, double-homozygous *srgp-1(gk441841); hmp-2(qm39)* embryos displayed 57.1% embryonic lethality, arresting with dorsal humps during elongation (Fig. 4B).

We next performed rescue experiments using SRGP-1 fragments in *srgp-1(gk441841); hmp-2(qm39)* embryos. SRGP-1(full-length)::GFP and SRGP-1(ΔGAP)::GFP were capable of strong rescue, although full-length SRGP-1::GFP rescued more effectively (Fig. 4C,D,G). Importantly, *srgp-1(gk441841); hmp-2(qm39); Ex[srgp-1(ΔC)::gfp]* embryos were indistinguishable from *srgp-1(gk441841); hmp-2(qm39)* alone (Fig. 4E,G), indicating that the C terminus of SRGP-1 is functionally important during elongation. The C terminus alone was

Development (2022) 149, dev200775. doi:10.1242/dev.200775

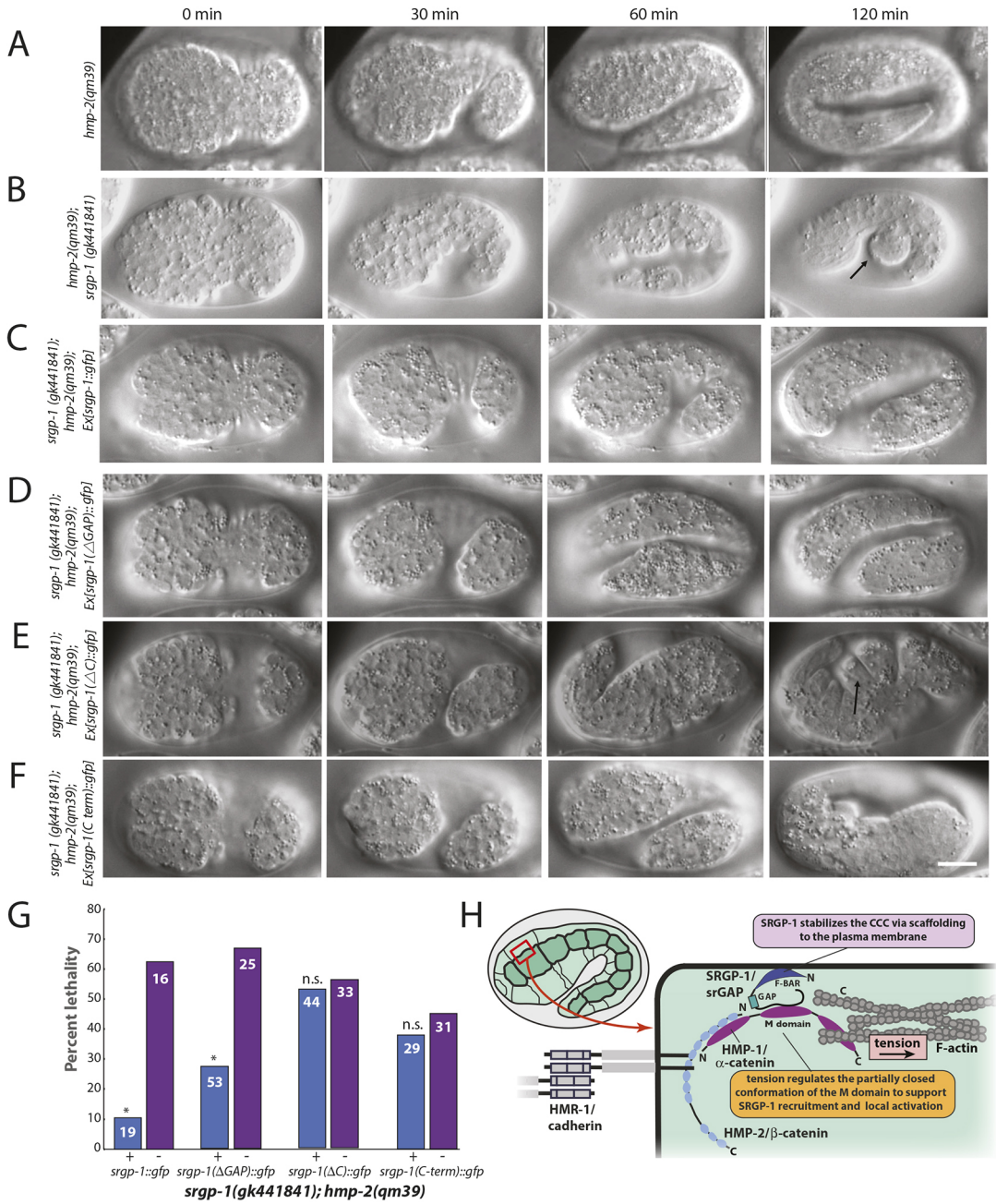

Fig. 4. The SRGP-1 C terminus is required for embryonic elongation in an adhesion-sensitized background. (A) In *hmp-2(qm39)* homozygotes, ventral enclosure and elongation proceed normally in almost all embryos. (B) Homozygous *hmp-2(qm39); srgp-1(gk441841)* embryos begin to fail at 120 min, and embryos form dorsal humps (arrow). (C) *srgp-1(gk441841); hmp-2(qm39); Ex[srgp-1::gfp]* embryos are mostly rescued. (D) *srgp-1(gk441841); hmp-2(qm39); Ex[srgp-1(ΔGAP)::gfp]* embryos appear largely wild type; some embryos die during elongation. (E) *srgp-1(gk441841); hmp-2(qm39); Ex[srgp-1(ΔC)::gfp]* embryos die with dorsal humps during elongation (black arrow, 120 min). (F) *srgp-1(gk441841); hmp-2(qm39); Ex[srgp-1(C term)::gfp]* embryos die similarly. Scale bar: 10 µm. (G) Quantification of rescue in *srgp-1(gk441841); hmp-2(qm39)* strains. In all cases, GFP-expressing embryos were compared with their non-expressing siblings. Embryos expressing full-length SRGP-1::GFP or SRGP-1(ΔGAP)::GFP have significantly less embryonic lethality than their non-expressing siblings, whereas embryos expressing SRGP-1(ΔC)::GFP and SRGP-1(C term)::GFP are not significantly different from siblings. *n* values indicated on each bar for each genotype; n.s., not significant; **P*<0.05 (Fisher's exact test). (H) Model for SRGP-1 function. SRGP-1 interacts with membrane lipids through its F-BAR domain (dark blue) and binds the M domain of HMP-1/α-catenin through its C terminus. Tension causes conformational changes in, but not full extension of, the M domain of HMP-1/α-catenin that promote SRGP-1 binding.

not sufficient to rescue lethality, however (Fig. 4F,G). Taken together with its inability to support normal junctional localization (see Figs 1 and 2), these data suggest that a key functional role for the SRGP-1 C terminus is to target SRGP-1 to and maintain it at the CCC.

SRGP-1 stabilizes cadherin-dependent adhesion during epidermal morphogenesis

Here, we demonstrated the importance of the SRGP-1 C terminus in binding the HMP-1 M domain, and, unexpectedly, that a partially closed conformation of the M domain is necessary for junctional

Development (2022) 149, dev200775. doi:10.1242/dev.200775

maintenance of SRGP-1 mediated via its C terminus. Junctional SRGP-1 is in turn crucial for epidermal morphogenesis in sensitized backgrounds.

Although roles for srGAPs outside of neural tissues are beginning to be recognized (reviewed by Lucas and Hardin, 2017), roles of srGAPs during epithelial morphogenesis are poorly understood. In cultured mammalian cells, srGAP1 is recruited to junctions by tyrosine non-phosphorylated cortactin, where it downregulates Rho activity via its GAP domain (Liang et al., 2017). There is no clear cortactin homolog in *C. elegans* (J.H., unpublished) and the SRGP-1 GAP domain is relatively unimportant for its roles in morphogenesis (Zaidel-Bar et al., 2010; present work). A parsimonious model for SRGP-1 recruitment to the CCC during embryonic elongation involves direct HMP-1 binding.

Given when C-terminal fragments of SRGP-1::GFP localize to junctions, increased interaction of the SRGP-1 C terminus with HMP-1 appears to occur at a time when adherens junctions are under increased, but not maximal, tension (Fig. 4H). This contrasts with vertebrate vinculin. Vinculin is recruited to the CCC via α-catenin under tension by exposing a binding site within α-catenin that is normally buried within its M domain (Choi et al., 2012; Huveneers and de Rooij, 2013; Yonemura et al., 2010). Maximal vinculin binding to mammalian αE-catenin is favored by complete unfurling of the αE-catenin M domain (Yao et al., 2014); salt bridge mutations in the M domain of αE-catenin thus activate it for vinculin binding (Choi et al., 2012; Huveneers et al., 2012; Ishiyama et al., 2013; Yonemura et al., 2010). In contrast, we have shown here that similar mutations in the HMP-1M domain lead to loss of SRGP-1 junctional recruitment via its C terminus. SRGP-1 may therefore bind the HMP-1M domain in an intermediate conformation under tension that precedes complete unfurling of its M domain. At higher tension states, when the M domain is fully extended, HMP-1 may recruit other binding partners. Rigorous testing of such a mechanism awaits further biophysical experiments to interrogate the possibility of such a 'conformational clutch'.

In contrast to the SRGP-1 C terminus, full-length SRGP-1 is retained at junctions in *hmp-1* salt bridge mutants, but it is lost when HMP-1 is absent or when the HMP-1M domain is deleted. Multiple domains of SRGP-1 may therefore recognize different conformational states of the HMP-1M domain. Alternatively, another junctional protein with which SRGP-1 interacts may be recruited in an HMP-1-dependent manner and is retained even when the HMP-1M domain is more fully extended.

We showed previously that N- and C-terminal fragments of SRGP-1 can bind *in vitro*, suggesting head-to-tail autoinhibition. Moreover, overexpression of a C-terminal truncation of SRGP-1 leads to excessive membrane tubulations (Zaidel-Bar et al., 2010). Here, we have shown that the SRGP-1 C terminus alone can associate with junctions, but is insufficient for function, and that the SRGP-1 F-BAR domain is necessary. An irenic model that harmonizes these data is that HMP-1 recruits SRGP-1, leading to highly local, restrained activation of the membrane binding activities of SRGP-1 when embryonic elongation begins. SRGP-1 may therefore be similar to vinculin and talin, which undergo autoinhibition in the cytosol that is thought to be relieved by interactions with binding partners at adhesion sites (Bakolitsa et al., 2004; Dedden et al., 2019).

In summary, our results identify previously unknown roles for SRGP-1 during cadherin-dependent epithelial morphogenetic events. It will be interesting to determine whether vertebrate srGAPs can interact similarly with a component of the CCC. Future experiments should continue to clarify how this multifunctional family of proteins contributes to cadherin-dependent adhesion during morphogenesis.

MATERIALS AND METHODS

Nematode strains and genetics

C. elegans strains were maintained using standard methods (Brenner, 1974). Bristol N2 was used as wild type. Ten outcrosses to N2 were performed to remove background mutations from the Million Mutation Project strain, VC30226, which carries the *srgp-1(gk441841)* allele (Thompson et al., 2013). See Table S2 for a full list of strains used in this study.

DIC imaging

Four-dimensional (4D) DIC movies were collected on either a Nikon Optiphot-2 connected to a QiCAM camera (QImaging) or an Olympus BX50 connected to a Scion CFW-1512M camera (Scion Corp.) using Micro-Manager software (v. 1.42) (Edelstein et al., 2010, 2014). ImageJ plugins (https://worms.zoology.wisc.edu/research/4d/4d.html) were used to compress and view DIC movies.

Confocal imaging

SRGP-1::GFP; HMP-1::mScarlet-I embryos were dissected from adult hermaphrodites and mounted onto 10% agar pads in M9 solution and imaged essentially as described (Zaidel-Bar et al., 2010). For fluorescence imaging, a Dragonfly 500 spinning disc confocal microscope (Andor), mounted on a Leica DMi8 microscope, equipped with a Zyla camera and controlled by Fusion software (Andor) was used to collect images using 0.5 µm slices with a 63×/1.3 NA glycerol Leica objective at 20°C.

FRAP

FRAP analysis was conducted on *z*-projections of 4D confocal movies composed of four *z*-positions spaced 0.18 µm apart. Embryos were aged between 1.5- and 1.75-fold. 4D movies were generated by photobleaching a region of interest for 3 s and images were collected at 2 s intervals thereafter. Photobleaching was performed using an Andor Mosaic DMD and imaging was performed on a Leica Dmi8 microscope with a Dragonfly spinning disk (Andor). Images were collected on a Zyla CMOS camera using Fusion software (Andor). Recovery curves were analyzed via single-exponential curve fitting using custom Jython scripts written for Fiji. Scripts are available at https://worms.zoology.wisc.edu/research/microscopy/4d.html.

Intensity analyses

To compare intensity, mean HMP-1 junctional signal was measured by tracing HMP-1::GFP junctional signal on *z*-projections of four focal planes spaced 0.18 µm apart in embryos between 1.5- and 1.75-fold. Intensity profiles were collected by drawing a 1-pixel-wide line between nuclei during elongation. Colocalization of HMP-1 and SRGP-1 was performed in Fiji using the Just Another Colocalization Plugin (JACoP; https://imagej.nih.gov/ij/plugins/track/jacop.html) (Bolte and Cordelieres, 2006). Four focal planes from 25 junctional segments were combined into single stacks for each genotype. Maximum intensity *z*-projections were obtained, and automated Costes thresholding within JACoP was visually confirmed in each case.

CRISPR

HMP-1::mScarlet-I and SRGP-1::mScarlet-I worms were generated by plasmid-based CRISPR/Cas9 (Dickinson et al., 2015) using repair templates cloned using SapTrap cloning (Schwartz and Jorgensen, 2016). Small substitution mutations were made by marker-free genome editing (Arribere et al., 2014). Guides, homology arms primers and single-stranded repair templates for all CRISPR/Cas9 editing can be found in Table S1.

Microinjection

For transgenic lines, 10 ng/µl of the transgene of interest, in addition to 20 ng/µl non-coding DNA (F35D3) and 80 ng/µl *rol-6(su1006)*, was injected into the gonads of *srgp-1(gk441841)* young adults, as described previously (Mello and Fire, 1995).

Development (2022) 149, dev200775. doi:10.1242/dev.200775

Injection RNAi was performed as previously described (Walston et al., 2004). dsRNAs were generated using an Ambion T7 and/or T3 MEGAscript kit; the template used was the *srgp-1* feeding clone from a feeding library (Kamath et al., 2003), and the template used for *hmp-1 (yk1315a06)* was obtained from Dr Yuji Kohara (NEXTDB, http://nematode.lab.nig.ac.jp/). 'Weak' injection RNAi was accomplished by injecting young adults with 1 µg/µl dsRNA into the pseudocoelom and imaging embryos 18 h after injection.

Protein expression and purification

GST- and SUMO-His-tagged proteins were expressed in BL21-Gold(DE3) *Escherichia coli* cells and purified as described (Maiden et al., 2013; Mayers et al., 2011). Cells were induced with 0.1 mM IPTG at 18°C for 16 h. Wash and elution buffers were as follows: GST wash (1× PBS, 500 mM NaCl, 0.1% Tween-20 and 1 mM DTT), GST elution (50 mM, Tris pH 8.0, 0.3% glutathione, 150 mM NaCl), His wash (50 mM sodium phosphate, pH 8.0, 300 mM NaCl, 0.1% Tween-20, 10 mM imidazole) and His elution (250 mM imidazole, 100 mM NaCl, 10% glycerol, 50 mM HEPES, pH 7.6).

DNA encoding wild-type full-length HMP-1 (aa1-927) and M region (aa270-646) and DNA encoding 551/554A mutant proteins was cloned into pMAL-c6t to make MBP-tagged fusion proteins. Fusion proteins were expressed in Novagen Rosetta DE3 competent *E. coli* cells (Sigma-Aldrich, 70954) and purified as described by Kwiatkowski et al., (2010) and Hansen et al. (2013). MBP-tagged proteins were bound to amylose-conjugated beads. Bound beads were then equilibrated in cleavage buffer (20 mM Tris, pH 8.0, 150 mM NaCl, 2 mM EDTA, 10% glycerol and 1 mM DTT) and incubated with tobacco etch virus protease overnight at 4°C to cleave proteins from the tag. Proteins were then purified by Mono Q ion-exchange chromatography at 4°C, followed by S200 gel-filtration chromatography at 4°C. Purified proteins were eluted in 20 mM Tris, pH 8.0, 150 mM NaCl, 10% glycerol and 1 mM DTT, concentrated to working concentrations using a Millipore column concentrator and flash-frozen in liquid nitrogen.

Directed yeast two-hybrid assays

Yeast two-hybrid assays were performed as described previously (Lynch et al., 2012). Either full-length HMP-1 or HMP-2 yeast two-hybrid plasmids (Kwiatkowski et al., 2010) were transformed into Y2H Gold yeast singly or with a plasmid encoding full-length SRGP-1 that was cloned into the pGBKT7 vector (Clontech). Positive single transformants were tested for autoactivation, and double transformants were patched onto SD/-Leu/-Trp/X-α-gal/AurA plates. Colonies that grew and turned blue were considered positive for a direct interaction.

Co-immunoprecipitation

C. elegans used for co-immunoprecipitations were grown in liquid culture as previously described (Stiernagle, 2006). Co-immunoprecipitations were carried out as previously described (Cox-Paulson et al., 2012). HMP-1 and HMP-2 were co-immunoprecipitated using a rabbit anti-HMP-1 antibody (Zaidel-Bar et al., 2010) as a control. Western blots were performed as described previously (Zhang et al., 2016), blotting with rabbit anti-GFP or rabbit anti-HMP-1 antibodies and using chemiluminescence to detect proteins using an Odyssey Fc imaging system (LI-COR Biosciences).

Feeding RNAi

L4 worms were transferred to plates seeded with *E. coli* expressing dsRNA from *let-502* or L4440 (control) vectors overnight. The following day, worms were cut open and their embryos were mounted, aged to 1.5 fold, and imaged.

Pull-down assays

Pull-downs between GST-SRGP-1 and His-SUMO-HMP-1 fragments were performed as described previously (Takahashi et al., 2015). Two replicates were performed in each case. When testing GST-SRGP-1 (C term) against His-SUMO-HMP-1 fragments, purified GST-SRGP-1 (C term) was incubated individually with His-SUMO-HMP-1 fragments still immobilized on Ni-NTA agarose resin for 1 h at 4°C. After washing five times with buffer (50 mM HEPES, pH 7.4; 1 mM EDTA, pH 8.0; 0.1 M KCl; 1 mM $MgCl_2$; 12.5% w/v glycerol), His elution was then carried out. Finally, eluates were run on SDS-PAGE gels and stained with Coomassie Brilliant Blue to visualize proteins.

Limited proteolysis

Proteins were diluted to 12 µM in 20 mM Tris, pH 8.0, 150 mM NaCl and 1 mM DTT and incubated at room temperature in 0.05 mg/ml sequencing grade trypsin (Roche Applied Science). Digestions were stopped with 2× Laemmli sample buffer followed by boiling. Samples were run by SDS-PAGE and then stained with 0.1% Coomassie Brilliant Blue R-250, 40% ethanol and 10% acetic acid. Gels were scanned on a LI-COR Odyssey FC scanner.

Statistical analysis

Fisher's Exact Test (http://www.graphpad.com/quickcalcs/contingency1/) was used to determine significance between rescue groups. Differences in cytoplasmic fluorescence levels were determined using one-way ANOVA with Tukey post-hoc testing for multiple comparisons or unpaired two-tailed Student's *t*-tests for single comparisons after measuring average junctional and cytoplasmic signals in ImageJ. Significant difference in Pearson's R for colocalizations was assessed using the online Z calculator available at https://www.calculator.net/z-score-calculator.html.

Acknowledgements

Some strains were provided by the *C. elegans* Genetics Center, which is funded by the NIH Office of Research Infrastructure Programs (P40 OD010440). A cDNA clone for *hmp-1 (yk1315a06)* was provided by Yuji Kohara (National Institute of Genetics, Japan). We are grateful to Seth Blair for the use of his LI-COR system.

Competing interests

The authors declare no competing or financial interests.

Author contributions

Conceptualization: J.M.S., B.L., J.H.; Methodology: J.M.S., B.L., S.C.T.M., X.S., J.H.; Software: J.H.; Validation: J.M.S., B.L.; Formal analysis: J.M.S., B.L., J.H.; Investigation: J.M.S., B.L., S.C.T.M., J.A.H.; Resources: J.M.S., B.L., X.S.; Writing - original draft: B.L.; Writing - review & editing: J.M.S., J.A.H., J.H.; Visualization: J.M.S., B.L., J.H.; Supervision: J.H.; Funding acquisition: J.H.

Funding

This work was supported by National Institute of General Medical Sciences grants (R01GM058038, R01GM127687 and R35GM145312 to J.H.). S.C.T.M. was supported by a Gilliam Fellowship from the Howard Hughes Medical Institute, by an Advanced Opportunities Fellowship and a COVID-19 dissertation completion fellowship from the University of Wisconsin-Madison. Deposited in PMC for release after 12 months.

Peer review history

The peer review history is available online at https://journals.biologists.com/dev/article-lookup/doi/10.1242/dev.200775.reviewer-comments.pdf.

References

Arribere, J. A., Bell, R. T., Fu, B. X., Artiles, K. L., Hartman, P. S. and Fire, A. Z. (2014). Efficient marker-free recovery of custom genetic modifications with CRISPR/Cas9 in Caenorhabditis elegans. *Genetics* **198**, 837-846. doi:10.1534/genetics.114.169730

Bakolitsa, C., Cohen, D. M., Bankston, L. A., Bobkov, A. A., Cadwell, G. W., Jennings, L., Critchley, D. R., Craig, S. W. and Liddington, R. C. (2004). Structural basis for vinculin activation at sites of cell adhesion. *Nature* **430**, 583-586. doi:10.1038/nature02610

Barrick, S., Li, J., Kong, X., Ray, A., Tajkhorshid, E. and Leckband, D. (2018). Salt bridges gate α-catenin activation at intercellular junctions. *Mol. Biol. Cell* **29**, 111-122. doi:10.1091/mbc.E17-03-0168

Bolte, S. and Cordelieres, F. P. (2006). A guided tour into subcellular colocalization analysis in light microscopy. *J. Microsc.* **224**, 213-232. doi:10.1111/j.1365-2818.2006.01706.x

Brenner, S. (1974). The genetics of *Caenorhabditis elegans*. *Genetics* **77**, 71-94. doi:10.1093/genetics/77.1.71

Buckley, C. D., Tan, J., Anderson, K. L., Hanein, D., Volkmann, N., Weis, W. I., Nelson, W. J. and Dunn, A. R. (2014). Cell adhesion. The minimal cadherin-

catenin complex binds to actin filaments under force. *Science* **346**, 1254211. doi:10.1126/science.1254211

Callaci, S., Morrison, K., Shao, X., Schuh, A. L., Wang, Y., Yates, J. R., Hardin, J. and Audhya, A. (2015). Phosphoregulation of the *C. elegans* cadherin-catenin complex. *Biochem. J.* **472**, 339-352. doi:10.1042/BJ20150410

Carlson, B. R., Lloyd, K. E., Kruszewski, A., Kim, I.-H., Rodriguiz, R. M., Heindel, C., Faytell, M., Dudek, S. M., Wetsel, W. C. and Soderling, S. H. (2011). WRP/srGAP3 facilitates the initiation of spine development by an inverse F-BAR domain, and its loss impairs long-term memory. *J. Neurosci.* **31**, 2447-2460. doi:10.1523/JNEUROSCI.4433-10.2011

Charras, G. and Yap, A. S. (2018). Tensile forces and mechanotransduction at cell-cell junctions. *Curr. Biol.* **28**, R445-R457. doi:10.1016/j.cub.2018.02.003

Chisholm, A. D. and Hardin, J. (2005). Epidermal morphogenesis. In *WormBook: the Online Review of C. elegans Biology*. doi:10.1895/wormbook.1.35.1

Choi, H. J., Pokutta, S., Cadwell, G. W., Bobkov, A. A., Bankston, L. A., Liddington, R. C. and Weis, W. I. (2012). αE-catenin is an autoinhibited molecule that coactivates vinculin. *Proc. Natl. Acad. Sci. USA* **109**, 8576-8581. doi:10.1073/pnas.1203906109

Costa, M., Raich, W., Agbunag, C., Leung, B., Hardin, J. and Priess, J. R. (1998). A putative catenin-cadherin system mediates morphogenesis of the Caenorhabditis elegans embryo. *J. Cell Biol.* **141**, 297-308. doi:10.1083/jcb.141.1.297

Coutinho-Budd, J., Ghukasyan, V., Zylka, M. J. and Polleux, F. (2012). The F-BAR domains from srGAP1, srGAP2 and srGAP3 regulate membrane deformation differently. *J. Cell Sci.* **125**, 3390-3401. doi:10.1242/jcs.098962

Cox-Paulson, E. A., Walck-Shannon, E., Lynch, A. M., Yamashiro, S., Zaidel-Bar, R., Eno, C. C., Ono, S. and Hardin, J. (2012). Tropomodulin protects alpha-catenin-dependent junctional-actin networks under stress during epithelial morphogenesis. *Curr. Biol.* **22**, 1500-1505. doi:10.1016/j.cub.2012.06.025

Dedden, D., Schumacher, S., Kelley, C. F., Zacharias, M., Biertumpfel, C., Fassler, R. and Mizuno, N. (2019). The architecture of Talin1 reveals an autoinhibition mechanism. *Cell* **179**, 120-131e13. doi:10.1016/j.cell.2019.08.034

Dickinson, D. J., Pani, A. M., Heppert, J. K., Higgins, C. D. and Goldstein, B. (2015). Streamlined genome engineering with a self-excising drug selection cassette. *Genetics* **200**, 1035-1049. doi:10.1534/genetics.115.178335

Edelstein, A., Amodaj, N., Hoover, K., Vale, R. and Stuurman, N. (2010). Computer control of microscopes using μManager. *Curr. Protoc. Mol. Biol.* **92**, 14.20.1-14.20.17. doi:10.1002/0471142727.mb1420s92

Edelstein, A. D., Tsuchida, M. A., Amodaj, N., Pinkard, H., Vale, R. D. and Stuurman, N. (2014). Advanced methods of microscope control using μManager software. *J. Biol. Methods* **1**, e10. doi:10.14440/jbm.2014.36

Endris, V., Haussmann, L., Buss, E., Bacon, C., Bartsch, D. and Rappold, G. (2011). SrGAP3 interacts with lamellipodin at the cell membrane and regulates Rac-dependent cellular protrusions. *J. Cell Sci.* **124**, 3941-3955. doi:10.1242/jcs.077081

Foletta, V. C., Brown, F. D. and Young III, W. S. (2002). Cloning of rat ARHGAP4/C1, a RhoGAP family member expressed in the nervous system that colocalizes with the Golgi complex and microtubules. *Brain Res. Mol. Brain Res.* **107**, 65-79. doi:10.1016/S0169-328X(02)00448-5

Guerrier, S., Coutinho-Budd, J., Sassa, T., Gresset, A., Jordan, N. V., Chen, K., Jin, W.-L., Frost, A. and Polleux, F. (2009). The F-BAR domain of srGAP2 induces membrane protrusions required for neuronal migration and morphogenesis. *Cell* **138**, 990-1004. doi:10.1016/j.cell.2009.06.047

Guez-Haddad, J., Sporny, M., Sasson, Y., Gevorkyan-Airapetov, L., Lahav-Mankovski, N., Margulies, D., Radzimanowski, J. and Opatowsky, Y. (2015). The neuronal migration factor srGAP2 achieves specificity in ligand binding through a two-component molecular mechanism. *Structure* **23**, 1989-2000. doi:10.1016/j.str.2015.08.009

Guillot, C. and Lecuit, T. (2013). Mechanics of epithelial tissue homeostasis and morphogenesis. *Science* **340**, 1185-1189. doi:10.1126/science.1235249

Hansen, S. D., Kwiatkowski, A. V., Ouyang, C. Y., Liu, H., Pokutta, S., Watkins, S. C., Volkmann, N., Hanein, D., Weis, W. I., Mullins, R. D. et al. (2013). αE-catenin actin-binding domain alters actin filament conformation and regulates binding of nucleation and disassembly factors. *Mol. Biol. Cell* **24**, 3710-3720. doi:10.1091/mbc.e13-07-0388

Harris, T. J. and Tepass, U. (2010). Adherens junctions: from molecules to morphogenesis. *Nat. Rev. Mol. Cell Biol.* **11**, 502-514. doi:10.1038/nrm2927

Heier, J. A., Pokutta, S., Dale, I. W., Kim, S. K., Hinck, A. P., Weis, W. I. and Kwiatkowski, A. V. (2021). Distinct intramolecular interactions regulate autoinhibition of vinculin binding in alphaT-catenin and alphaE-catenin. *J. Biol. Chem.*, **296**, 100582. doi:10.1016/j.jbc.2021.100582

Huveneers, S. and de Rooij, J. (2013). Mechanosensitive systems at the cadherin-F-actin interface. *Journal of Cell Science* **126**, 403-413. doi:10.1242/jcs.109447

Huveneers, S., Oldenburg, J., Spanjaard, E., van der Krogt, G., Grigoriev, I., Akhmanova, A., Rehmann, H. and de Rooij, J. (2012). Vinculin associates with endothelial VE-cadherin junctions to control force-dependent remodeling. *J. Cell Biol.* **196**, 641-652. doi:10.1083/jcb.201108120

Ishiyama, N., Tanaka, N., Abe, K., Yang, Y. J., Abbas, Y. M., Umitsu, M., Nagar, B., Bueler, S. A., Rubinstein, J. L., Takeichi, M. et al. (2013). An autoinhibited structure of α-catenin and its implications for vinculin recruitment to adherens junctions. *J. Biol. Chem.* **288**, 15913-15925. doi:10.1074/jbc.M113.453928

Ishiyama, N., Sarpal, R., Wood, M. N., Barrick, S. K., Nishikawa, T., Hayashi, H., Kobb, A. B., Flozak, A. S., Yemelyanov, A., Fernandez-Gonzalez, R. et al. (2018). Force-dependent allostery of the α-catenin actin-binding domain controls adherens junction dynamics and functions. *Nat. Commun.* **9**, 5121. doi:10.1038/s41467-018-07481-7

Kamath, R. S., Fraser, A. G., Dong, Y., Poulin, G., Durbin, R., Gotta, M., Kanapin, A., Le Bot, N., Moreno, S., Sohrmann, M. et al. (2003). Systematic functional analysis of the Caenorhabditis elegans genome using RNAi. *Nature* **421**, 231-237. doi:10.1038/nature01278

Kang, H., Bang, I., Jin, K. S., Lee, B., Lee, J., Shao, X., Heier, J. A., Kwiatkowski, A. V., Nelson, W. J., Hardin, J. et al. (2017). Structural and functional characterization of Caenorhabditis elegans alpha-catenin reveals constitutive binding to β-catenin and F-actin. *J. Biol. Chem.* **292**, 7077-7086. doi:10.1074/jbc.M116.769778

Kim, T.-J., Zheng, S., Sun, J., Muhamed, I., Wu, J., Lei, L., Kong, X., Leckband, D. E. and Wang, Y. (2015). Dynamic visualization of alpha-catenin reveals rapid, reversible conformation switching between tension states. *Curr. Biol.* **25**, 218-224. doi:10.1016/j.cub.2014.11.017

Kwiatkowski, A. V., Maiden, S. L., Pokutta, S., Choi, H. J., Benjamin, J. M., Lynch, A. M., Nelson, W. J., Weis, W. I. and Hardin, J. (2010). In vitro and in vivo reconstitution of the cadherin-catenin-actin complex from Caenorhabditis elegans. *Proc. Natl. Acad. Sci. USA* **107**, 14591-14596. doi:10.1073/pnas.1007349107

Leckband, D. E. and de Rooij, J. (2014). Cadherin adhesion and mechanotransduction. *Annu. Rev. Cell Dev. Biol.* **30**, 291-315. doi:10.1146/annurev-cellbio-100913-013212

Lecuit, T. and Yap, A. S. (2015). E-cadherin junctions as active mechanical integrators in tissue dynamics. *Nat. Cell Biol.* **17**, 533-539. doi:10.1038/ncb3136

Lecuit, T., Lenne, P.-F. and Munro, E. (2011). Force generation, transmission, and integration during cell and tissue morphogenesis. *Annu. Rev. Cell Dev. Biol.* **27**, 157-184. doi:10.1146/annurev-cellbio-100109-104027

Li, J., Newhall, J., Ishiyama, N., Gottardi, C., Ikura, M., Leckband, D. E. and Tajkhorshid, E. (2015). Structural determinants of the mechanical stability of α-catenin. *J. Biol. Chem.* **290**, 18890-18903. doi:10.1074/jbc.M115.647941

Liang, X., Budnar, S., Gupta, S., Verma, S., Han, S. P., Hill, M. M., Daly, R. J., Parton, R. G., Hamilton, N. A., Gomez, G. A. et al. (2017). Tyrosine dephosphorylated cortactin downregulates contractility at the epithelial zonula adherens through SRGAP1. *Nat. Commun.* **8**, 790. doi:10.1038/s41467-017-00797-w

Lockwood, C., Zaidel-Bar, R. and Hardin, J. (2008). The *C. elegans* zonula occludens ortholog cooperates with the cadherin complex to recruit actin during morphogenesis. *Curr. Biol.* **18**, 1333-1337. doi:10.1016/j.cub.2008.07.086

Lucas, B. and Hardin, J. (2017). Mind the (sr)GAP – roles of Slit-Robo GAPs in neurons, brains and beyond. *J. Cell Sci.* **130**, 3965-3974. doi:10.1242/jcs.207456

Lynch, A. M., Grana, T., Cox-Paulson, E., Couthier, A., Cameron, M., Chin-Sang, I., Pettitt, J. and Hardin, J. (2012). A genome-wide functional screen shows MAGI-1 is an L1CAM-dependent stabilizer of apical junctions in *C. elegans*. *Curr. Biol.* **22**, 1891-1899. doi:10.1016/j.cub.2012.08.024

Maiden, S. L. and Hardin, J. (2011). The secret life of alpha-catenin: moonlighting in morphogenesis. *J. Cell Biol.* **195**, 543-552. doi:10.1083/jcb.201103106

Maiden, S. L., Harrison, N., Keegan, J., Cain, B., Lynch, A. M., Pettitt, J. and Hardin, J. (2013). Specific conserved C-terminal amino acids of *Caenorhabditis elegans* HMP-1/α-catenin modulate F-actin binding independently of vinculin. *J. Biol. Chem.* **288**, 5694-5706. doi:10.1074/jbc.M112.438093

Marston, D. J. and Goldstein, B. (2006). Actin-based forces driving embryonic morphogenesis in Caenorhabditis elegans. *Curr. Opin. Genet. Dev.* **16**, 392-398. doi:10.1016/j.gde.2006.06.002

Marston, D. J., Higgins, C. D., Peters, K. A., Cupp, T. D., Dickinson, D. J., Pani, A. M., Moore, R. P., Cox, A. H., Kiehart, D. P. and Goldstein, B. (2016). MRCK-1 drives apical constriction in *C. elegans* by linking developmental patterning to force generation. *Curr. Biol.* **26**, 2079-2089. doi:10.1016/j.cub.2016.06.010

Mason, F. M., Heimsath, E. G., Higgs, H. N. and Soderling, S. H. (2011). Bi-modal regulation of a formin by srGAP2. *J. Biol. Chem.* **286**, 6577-6586. doi:10.1074/jbc.M110.190397

Mayers, J. R., Fyfe, I., Schuh, A. L., Chapman, E. R., Edwardson, J. M. and Audhya, A. (2011). ESCRT-0 assembles as a heterotetrameric complex on membranes and binds multiple ubiquitinylated cargoes simultaneously. *J. Biol. Chem.* **286**, 9636-9645. doi:10.1074/jbc.M110.185363

Mege, R. M. and Ishiyama, N. (2017). Integration of cadherin adhesion and cytoskeleton at adherens junctions. *Cold Spring Harb. Perspect. Biol.* **9**, a028738. doi:10.1101/cshperspect.a028738

Mello, C. and Fire, A. (1995). DNA transformation. In *Caenorhabditis elegans: Modern Biological Analysis of an Organism*, pp. 451-482. Elsevier BV.

Neukomm, L. J., Frei, A. P., Cabello, J., Kinchen, J. M., Zaidel-Bar, R., Ma, Z., Haney, L. B., Hardin, J., Ravichandran, K. S., Moreno, S. et al. (2011). Loss of the RhoGAP SRGP-1 promotes the clearance of dead and injured cells in *Caenorhabditis elegans*. *Nat. Cell Biol.* **13**, 79-86. doi:10.1038/ncb2138

Niessen, C. M., Leckband, D. and Yap, A. S. (2011). Tissue organization by cadherin adhesion molecules: dynamic molecular and cellular mechanisms of morphogenetic regulation. *Physiol. Rev.* **91**, 691-731. doi:10.1152/physrev.00004.2010

Pang, S. M., Le, S., Kwiatkowski, A. V. and Yan, J. (2019). Mechanical stability of alphaT-catenin and its activation by force for vinculin binding. *Mol. Biol. Cell* **30**, 1930-1937. doi:10.1091/mbc.E19-02-0102

Pannekoek, W. J., de Rooij, J. and Gloerich, M. (2019). Force transduction by cadherin adhesions in morphogenesis. *F1000Res* **8**, 1044. doi:10.12688/f1000research.18779.1

Pinheiro, D. and Bellaiotache, Y. (2018). Mechanical force-driven adherens junction remodeling and epithelial dynamics. *Developmental Cell* **47**, 391. doi:10.1016/j.devcel.2018.10.021

Pokutta, S. and Weis, W. I. (2000). Structure of the dimerization and beta-catenin-binding region of alpha-catenin. *Mol. Cell* **5**, 533-543. doi:10.1016/S1097-2765(00)80447-5

Pokutta, S. and Weis, W. I. (2007). structure and mechanism of cadherins and catenins in cell-cell contacts. *Annu. Rev. Cell Dev. Biol.*, **23**, 237-261. doi:10.1146/annurev.cellbio.22.010305.104241

Priya, R. and Yap, A. S. (2015). Active tension: the role of cadherin adhesion and signaling in generating junctional contractility. *Curr. Top. Dev. Biol.* **112**, 65-102. doi:10.1016/bs.ctdb.2014.11.016

Schwartz, M. L. and Jorgensen, E. M. (2016). SapTrap, a toolkit for high-throughput CRISPR/Cas9 gene modification in Caenorhabditis elegans. *Genetics* **202**, 1277-1288. doi:10.1534/genetics.115.184275

Shao, X., Lucas, B., Strauch, J. and Hardin, J. (2019). The adhesion modulation domain of Caenorhabditis elegans α-catenin regulates actin binding during morphogenesis. *Mol. Biol. Cell* **30**, 2115-2123. doi:10.1091/mbc.E19-01-0018

Soderling, S. H., Binns, K. L., Wayman, G. A., Davee, S. M., Ong, S. H., Pawson, T. and Scott, J. D. (2002). The WRP component of the WAVE-1 complex attenuates Rac-mediated signalling. *Nat. Cell Biol.* **4**, 970-975. doi:10.1038/ncb886

Sporny, M., Guez-Haddad, J., Kreusch, A., Shakartzi, S., Neznansky, A., Cross, A., Isupov, M. N., Qualmann, B., Kessels, M. M. and Opatowsky, Y. (2017). Structural history of human SRGAP2 proteins. *Mol Biol Evol* **34**, 1463-1478. doi:10.1093/molbev/msx094

Stiernagle, T. (2006). Maintenance of *C. elegans*. In *WormBook: the Online Review of C. elegans Biology*. doi:10.1895/wormbook.1.101.1

Takahashi, H., Mayers, J. R., Wang, L., Edwardson, J. M. and Audhya, A. (2015). Hrs and STAM function synergistically to bind ubiquitin-modified cargoes in vitro. *Biophys J* **108**, 76-84. doi:10.1016/j.bpj.2014.11.004

Takeichi, M. (2014). Dynamic contacts: rearranging adherens junctions to drive epithelial remodelling. *Nat. Rev. Mol. Cell Biol.* **15**, 397-410. doi:10.1038/nrm3802

Thompson, O., Edgley, M., Strasbourger, P., Flibotte, S., Ewing, B., Adair, R., Au, V., Chaudhry, I., Fernando, L., Hutter, H. et al. (2013). The million mutation project: a new approach to genetics in Caenorhabditis elegans. *Genome Res.* **23**, 1749-1762. doi:10.1101/gr.157651.113

Vuong-Brender, T. T., Yang, X. and Labouesse, M. (2016). *C. elegans* embryonic morphogenesis. *Curr. Top. Dev. Biol.* **116**, 597-616. doi:10.1016/bs.ctdb.2015.11.012

Vuong-Brender, T. T., Ben Amar, M., Pontabry, J. and Labouesse, M. (2017). The interplay of stiffness and force anisotropies drives embryo elongation. *eLife* **6**, e23866. doi:10.7554/eLife.23866

Vuong-Brender, T. T. K., Boutillon, A., Rodriguez, D., Lavilley, V. and Labouesse, M. (2018). HMP-1/alpha-catenin promotes junctional mechanical integrity during morphogenesis. *PLoS One* **13**, e0193279. doi:10.1371/journal.pone.0193279

Walck-Shannon, E. and Hardin, J. (2014). Cell intercalation from top to bottom. *Nat. Rev. Mol. Cell. Biol.* **15**, 34-48. doi:10.1038/nrm3723

Walston, T., Tuskey, C., Edgar, L., Hawkins, N., Ellis, G., Bowerman, B., Wood, W. and Hardin, J. (2004). Multiple Wnt signaling pathways converge to orient the mitotic spindle in early *C. elegans* embryos. *Dev. Cell* **7**, 831-841. doi:10.1016/j.devcel.2004.10.008

Waltereit, R., Leimer, U., Halbach, O. V. U., Panke, J., Holter, S. M., Garrett, L., Wittig, K., Schneider, M., Schmitt, C., Calzada-Wack, J. et al. (2012). Srgap3(-/-) mice present a neurodevelopmental disorder with schizophrenia-related intermediate phenotypes. *FASEB J.* **26**, 4418-4428. doi:10.1096/fj.11-202317

Williams-Masson, E. M., Malik, A. N. and Hardin, J. (1997). An actin-mediated two-step mechanism is required for ventral enclosure of the *C. elegans* hypodermis. *Development* **124**, 2889-2901. doi:10.1242/dev.124.15.2889

Wong, K., Ren, X.-R., Huang, Y.-Z., Xie, Y., Liu, G., Saito, H., Tang, H., Wen, L., Brady-Kalnay, S. M., Mei, L. et al. (2001). Signal transduction in neuronal migration: roles of GTPase activating proteins and the small GTPase Cdc42 in the Slit-Robo pathway. *Cell* **107**, 209-221. doi:10.1016/S0092-8674(01)00530-X

Xu, X. P., Pokutta, S., Torres, M., Swift, M. F., Hanein, D., Volkmann, N. and Weis, W. I. (2020). Structural basis of alphaE-catenin-F-actin catch bond behavior. *eLife* **9**, e60878. doi:10.7554/eLife.60878

Yamazaki, D., Itoh, T., Miki, H. and Takenawa, T. (2013). srGAP1 regulates lamellipodial dynamics and cell migratory behavior by modulating Rac1 activity. *Mol. Biol. Cell* **24**, 3393-3405. doi:10.1091/mbc.e13-04-0178

Yang, Y., Marcello, M., Endris, V., Saffrich, R., Fischer, R., Trendelenburg, M. F., Sprengel, R. and Rappold, G. (2006). MEGAP impedes cell migration via regulating actin and microtubule dynamics and focal complex formation. *Exp. Cell. Res.* **312**, 2379-2393. doi:10.1016/j.yexcr.2006.04.001

Yao, M., Qiu, W., Liu, R., Efremov, A. K., Cong, P., Seddiki, R., Payre, M., Lim, C. T., Ladoux, B., Mège, R.-M. et al. (2014). Force-dependent conformational switch of alpha-catenin controls vinculin binding. *Nat. Commun.* **5**, 4525. doi:10.1038/ncomms5525

Yonemura, S., Wada, Y., Watanabe, T., Nagafuchi, A. and Shibata, M. (2010). α-Catenin as a tension transducer that induces adherens junction development. *Nat. Cell Biol.* **12**, 533-542. doi:10.1038/ncb2055

Zaidel-Bar, R., Joyce, M. J., Lynch, A. M., Witte, K., Audhya, A. and Hardin, J. (2010). The F-BAR domain of SRGP-1 facilitates cell-cell adhesion during *C. elegans* morphogenesis. *J. Cell Biol.* **191**, 761-769. doi:10.1083/jcb.201005082

Zhang, Y., Wang, X., Matakatsu, H., Fehon, R. and Blair, S. S. (2016). The novel SH3 domain protein Dlish/CG10933 mediates fat signaling in *Drosophila* by binding and regulating Dachs. *eLife* **5**, e16624. doi:10.7554/eLife.16624

A

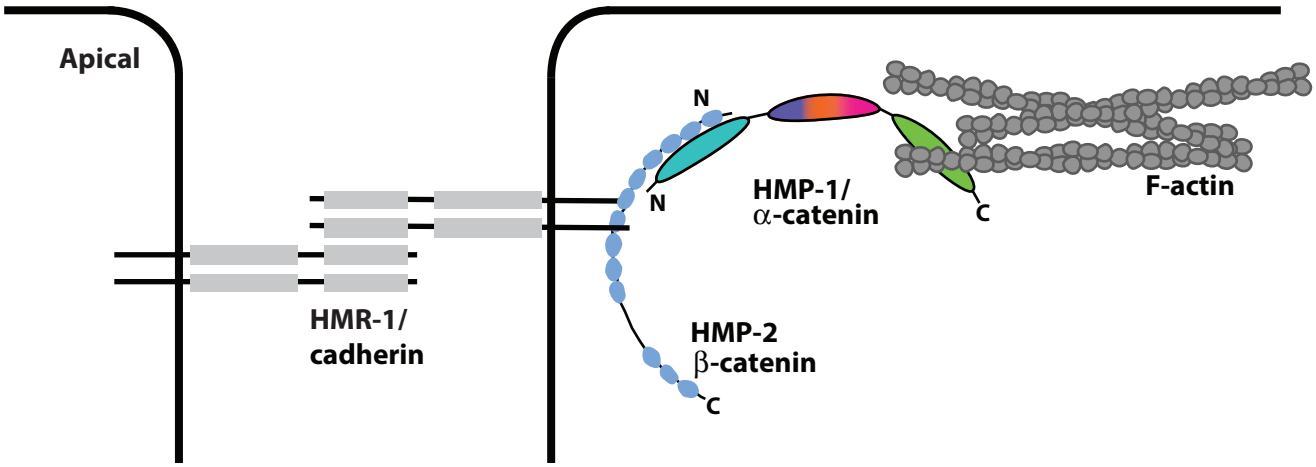

B

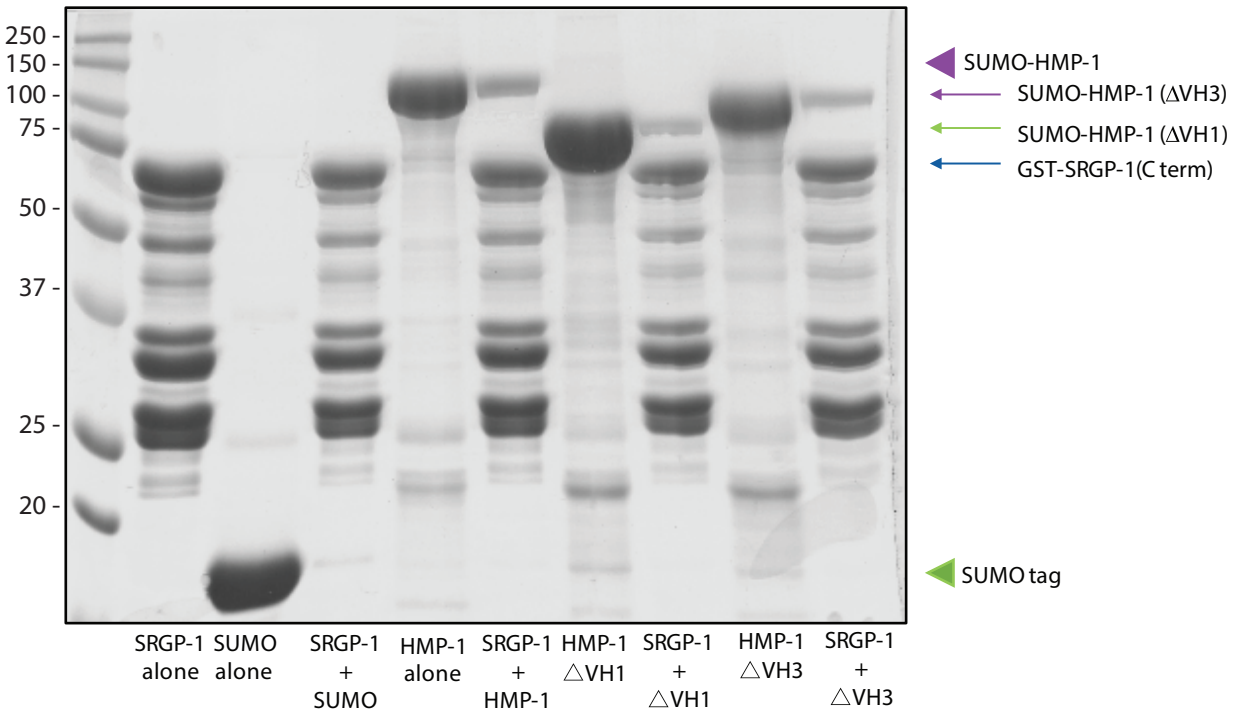

Fig. S1. The Vinculin Homology domain 2 (VH2) of HMP-1/α-catenin is crucial for the interaction with SRGP-1. (A) *C. elegans* has a well-conserved cadherin-catenin complex. HMR-1/cadherin (light grey) forms calcium-dependent, homophilic bonds between cells, and its C-terminal tail binds HMP-2/β-catenin (light blue) in the cytoplasm. HMP-2/β-catenin binds the N terminusthe HMP-1/α-catenin (cyan) which interacts with F-actin (dark grey) through its C-terminal actin-binding domain (green). (B) GST-SRGP-1(C-term) (blue arrow) pulls down SUMO-HMP-1 constructs that contain the VH2 domain but not the SUMO tag alone (green arrowhead).

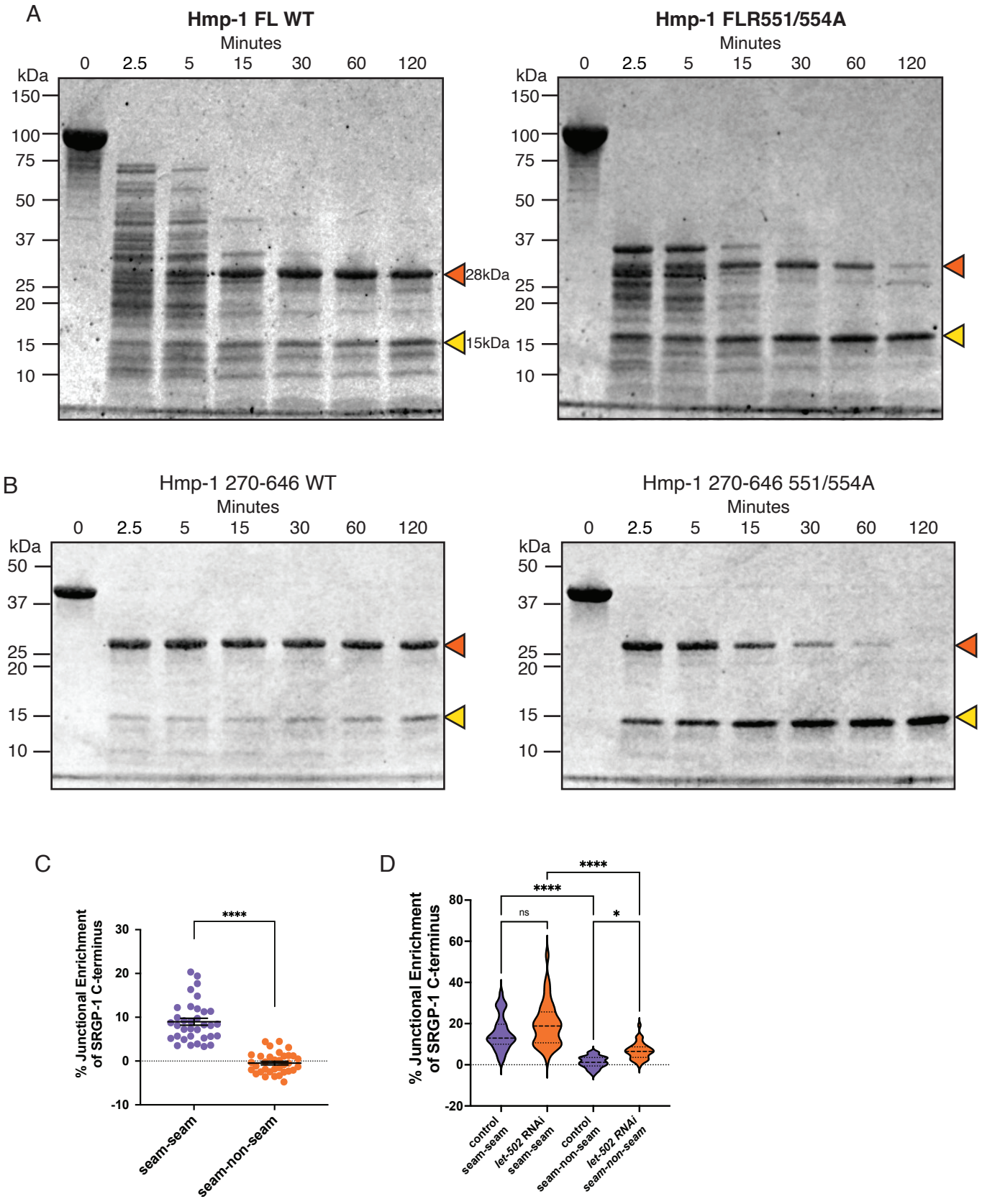

Fig. S2. Salt bridge mutations open the HMP-1 M-region. (A) Trypsin limited proteolysis of full-length wild-type and 551/554A mutant HMP-1. A stable fragment at 28kDa (orange arrow) is present with a minor stable fragment at 15kDa (yellow arrow). In the case of the 551/554A mutant protein, the 28kDa fragment is less stable and more of the smaller 15kDa species accumulates, indicating that the 551/554A mutant is more open and susceptible to trypsin digestion. (B) Limited proteolysis of wild-type and 551/554A mutant HMP-1 M domain. The same fragments at 28kDa (orange arrow) a 15kDa (yellow arrow) are present. As with the full-length proteins, in the case of the 551/554A M domain the 28kDa fragment is less stable and more of the smaller 15kDa species accumulates. (C) Junctional enrichment of SRGP-1(C)::GFP at seam-seam and seam-non-seam junctions (n=34 for both groups). (D) Junctional enrichment of SRGP-1(C)::GFP at seam-seam and seam-non-seam junctions in control RNAi or *let-502(RNAi)* embryos. Seam-seam control, n=29; seam-non-seam control, n=29; seam-seam *let-502*, n=38; seam-non-seam *let-502*, n=38.

Table S1. Primer sequences for CRISPR experiments performed in this study. See Materials and Methods for additional details.

hmp-1 C-terminal 5' Homology arm Forward Primer	5'-ggcacgtagctgccattgtc-3'
hmp-1 C-terminal 5' Homology arm Reverse Primer	5'-TAAACGACCGTTTATTCTTTGTTGATGGCGGCGATCAAGTTCTTC-3'
hmp-1 C-terminal 3' Homology arm Forward Primer	5'-TAGataatttatttcagttttattcatgtatcttcatacttttcc-3'
hmp-1 C-terminal 3' Homology arm Reverse Primer	5'-gaagcgaaaacatgggtgg-3'
hmp-1 C-terminal sgRNA	5'-GGGTCGTGATAGTGACGACG-3'
hmp-1 salt bridge sgRNA	5'-CATCGACAACGTCACAGACT-3'
hmp-1 salt bridge repair template	5'-GAAAATGCGGCCAACTGTGAAACTGTCGACTGTGCTGCCGGATCGATACGTGGAGCT GCTCTCGCTGTCTGTGACGTTGTCGATGCTGAAATGGACTTCCTTCAGAACTCTGAATAC-3'
srgp-1 C-terminal 5' Homology arm Forward Primer	5'-CACTGAGAGATCAGCTTCAGTTGATG-3'
srgp-1 C-terminal 5' Homology arm Reverse Primer	5'-TGGGCTGATGCTTGTCGCC-3'
srgp-1 C-terminal 3' Homology arm Forward Primer	5'-TGAtagttttggctgcgtct-3'
srgp-1 C-terminal 3' Homology arm Reverse Primer	5'-ggattttgtaaccgaacacttcc-3'
srgp-1 C-terminal sgRNA	5'-agacgcagccaaaactaTCA-3'

Table S2. Strains used in this study.

Click here to download Table S2

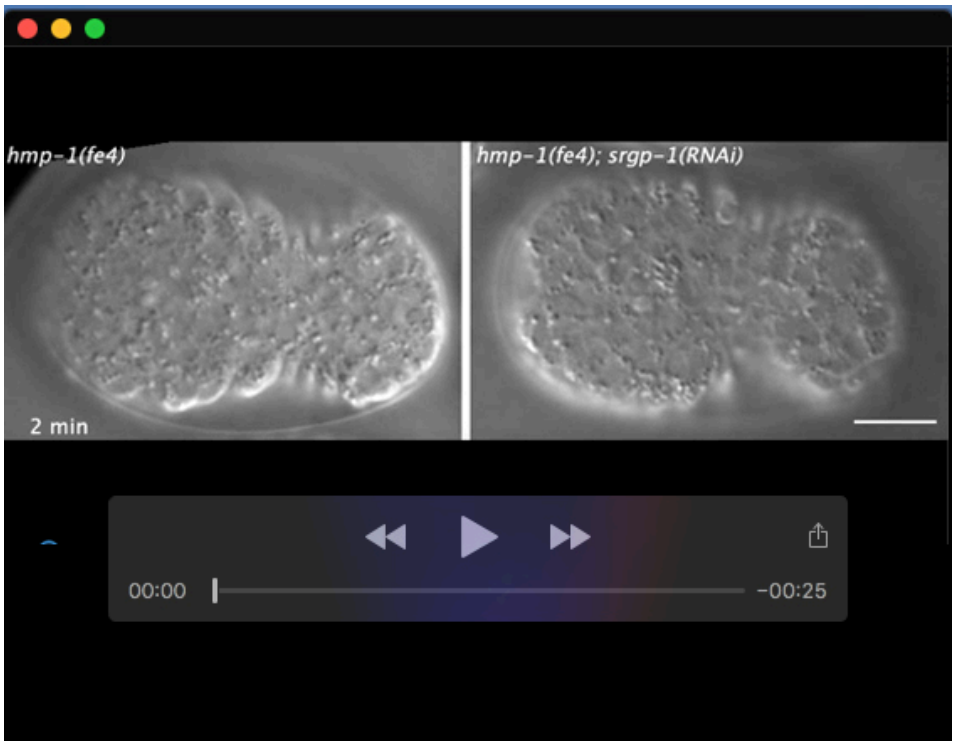

Movie 1. Movies corresponding to still images in Figure 3E. Elongation in *hmp-1(fe4)* and *hmp-1(fe4);srgp-1(RNAi)* embryos visualized using 4d DIC microscopy. Scale bar = 10 µm.